Article

Molecular Cell

RNA Remodeling Activity of DEAD Box Proteins Tuned by Protein Concentration, RNA Length, and ATP

Graphical Abstract

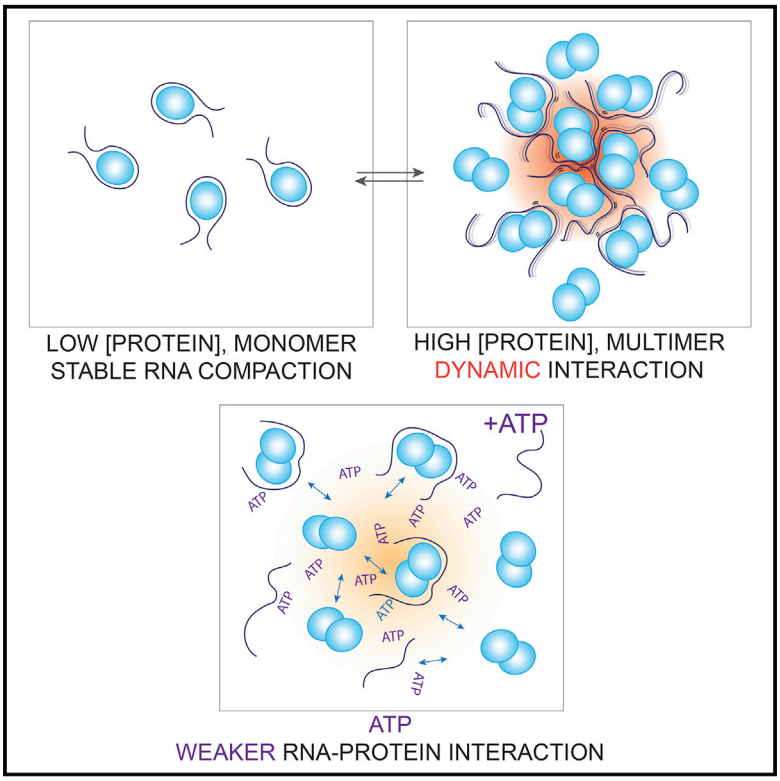

Authors

Younghoon Kim, Sua Myong

Correspondence

smyong@jhu.edu

In Brief

Kim et al. demonstrate that the RNA remodeling activity of DEAD box helicases is modulated by protein concentration, RNA length, and ATP. Their work suggests a plausible mechanism by which the RNP dynamic equilibrium is established and maintained to influence the fluidity of RNP droplets.

Highlights

- LAF-1 and DDX3X induce tight compaction of single-stranded RNA at low concentrations
- At high concentrations, LAF-1 forms a dimer and dynamically interacts with RNA.
- Dynamic RNA-protein interaction stimulates RNA annealing activity
- ATP modulates RNA remodeling activity by reducing affinity, dynamics, and annealing

Kim & Myong, 2016, Molecular Cell *63*, 865–876
September 1, 2016
http://dx.doi.org/10.1016/j.molcel.2016.07.010

CellPress

Molecular Cell
Article

RNA Remodeling Activity of DEAD Box Proteins Tuned by Protein Concentration, RNA Length, and ATP

Younghoon Kim[1] and Sua Myong[2,3,*]
[1]Bioengineering Department, University of Illinois, 1304 West Springfield Avenue, Urbana, IL 61801, USA
[2]Biophysics Department, Johns Hopkins University, 3400 North Charles Street, Baltimore, MD 21218, USA
[3]Physics Frontier Center (Center for Physics of Living Cells), University of Illinois, 1110 West Green Street, Urbana, IL 61801, USA
*Correspondence: smyong@jhu.edu
http://dx.doi.org/10.1016/j.molcel.2016.07.010

SUMMARY

DEAD box RNA helicases play central roles in RNP biogenesis. We reported earlier that LAF-1, a DEAD box RNA helicase in *C. elegans*, dynamically interacts with RNA and that the interaction likely contributes to the fluidity of RNP droplets. Here we investigate the molecular basis of the interaction of RNA with LAF-1 and its human homolog, DDX3X. We show that both LAF-1 and DDX3X, at low concentrations, are monomers that induce tight compaction of single-stranded RNA. At high concentrations, the proteins are multimeric and dynamically interact with RNA in an RNA length-dependent manner. The dynamic LAF-1-RNA interaction stimulates RNA annealing activity. ATP adversely affects the RNA remodeling ability of LAF-1 by suppressing the affinity, dynamics, and annealing activity of LAF-1, suggesting that ATP may promote disassembly of the RNP complex. Based on our results, we postulate a plausible molecular mechanism underlying the dynamic equilibrium of the LAF-1 RNP complex.

INTRODUCTION

LAF-1 and DDX3X are orthologous DEAD box RNA helicases found in *C. elegans* and humans, respectively. They belong to the DDX3 subfamily (Figure 1A) and are core protein components of ribonucleoprotein (RNP) bodies known as P granules (Updike and Strome, 2010). The helicases in the DDX3 subfamily, including LAF-1 (*C. elegans*), Ded1p (yeast), and Belle (*Drosophila*), play a role in RNP assembly and remodeling (Beckham et al., 2008; Shih et al., 2012; Yarunin et al., 2011). Our previous study demonstrated that a dynamic LAF-1-RNA interaction may be involved in the phase separation of RNP granules in vitro (Elbaum-Garfinkle et al., 2015). Both LAF-1 and DDX3X consist of a DEAD box helicase core and long stretches of flexible amino acids chains in their N-terminal domain (NTD) and C-terminal domain (CTD). Motif analysis defines characteristic amino acid sequences at both the NTD and CTD as intrinsically disordered regions (IDRs) (Goujon et al., 2010; Sigrist et al., 2013; Figures 1B and 1C). The IDRs on RNA binding proteins have been shown to guide the targeting of particular proteins, TIA and FUS, to stress granules (Gilks et al., 2004; Kato et al., 2012) and promote P body formation in yeast (Decker et al., 2007; Reijns et al., 2008). Because of the known propensity of IDRs to self-assemble, they have been proposed to play a major role in stimulating RNP granule assembly (Buchan, 2014), which is believed to occur spontaneously when the constituent components reach a critical concentration (Brangwynne et al., 2011). Interestingly, RNP granules display a liquid-like behavior (Brangwynne et al., 2009; Feric and Brangwynne, 2013; Wippich et al., 2013). Numerous recent studies demonstrated that liquid-like phase-separated granules formed with RNA binding proteins harboring intrinsically disordered or low-complexity domains that are implicated in neurodegenerative diseases. (Burke et al., 2015; Lin et al., 2015; Molliex et al., 2015; Patel et al., 2015; Zhang et al., 2015). Some of these proteins, including the ones with patients' mutations exhibit liquid-to-solid transition over time, recapitulating a pathological fibrillation observed in patients with neurodegenerative diseases such as amyotrophic lateral sclerosis (ALS) and frontotemporal dementia (FTD). A recent proteomics study reported that stress granules undergo a highly dynamic exchange at the surface, likely by forming an outer shell that surrounds a more stable core. This study demonstrated the role of ATP in both assembly and dynamics of RNP granules (Jain et al., 2016). Despite the emerging view on RNP formation and dynamics, the molecular details are unclear. Here we chose two key proteins found in RNP granules, LAF-1 and DDX3X, as model systems to dissect RNA-protein, protein-protein, and RNP-RNP interactions and thus elucidate the underlying molecular events that may contribute to RNP granule formation and dynamics.

The helicase core domain in the center of both LAF-1 and DDX3 features a Q motif containing the DEAD box peptide sequence and contains the ATP- and RNA-binding sites. Based on previous structural studies (Sengoku et al., 2006), we expect that the helicase core that consists of two RecA-like domains will interact with single-stranded RNA (ssRNA). However, the functional significance of the IDRs at both the N and C termini of LAF-1 and DDX3 is still poorly understood. The NTD of LAF-1 has an unusually high number of RGG/RG boxes that are known to bind ssRNA (Mattaj, 1993). In addition, the NTDs of both proteins consist of multiple consecutive sequence patches that are

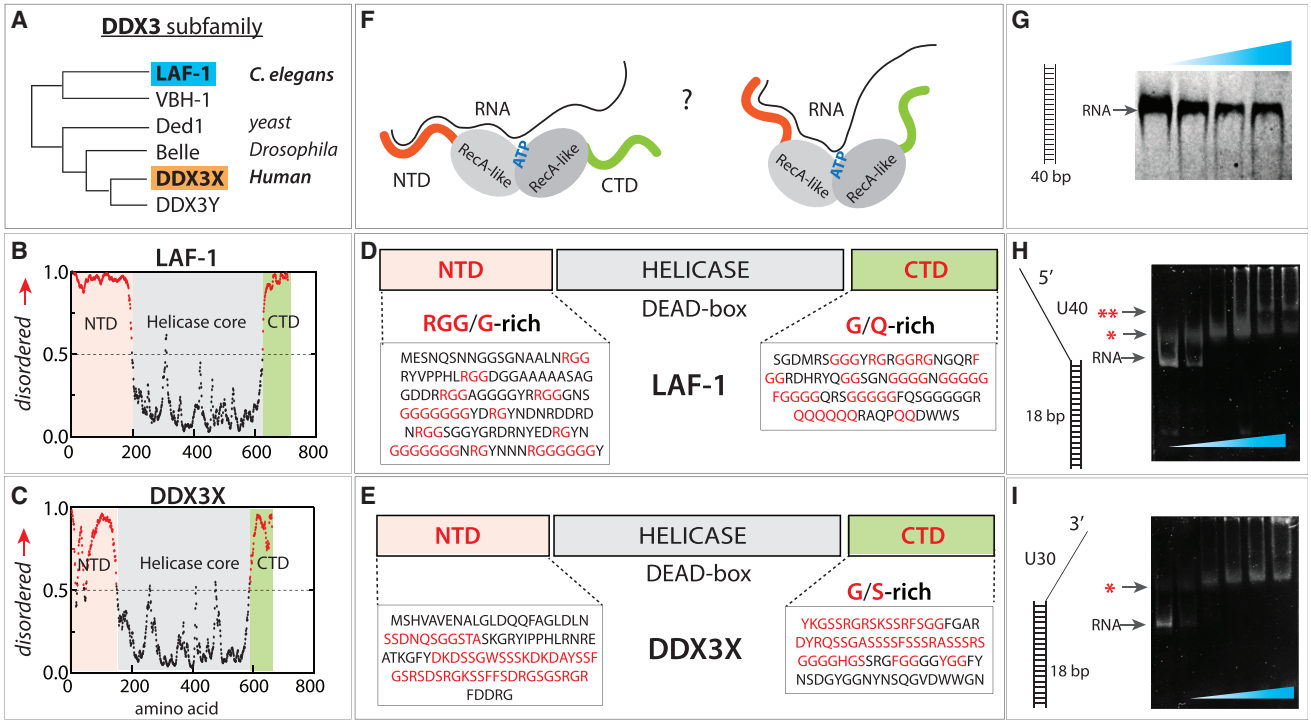

Figure 1. Domain Composition of LAF-1 and DDX3X

(A) DDX3 subfamily phylogeny.

(B and C) Analysis of the intrinsically disordered domains of LAF-1 (B) and DDX3X (C).

(D and E) Composition of LAF-1 and DDX3X containing intrinsically disordered N- and C-terminal domains and central helicase.

(F) Unknown protein-RNA interface between LAF-1 and RNA.

(G) EMSA showing no LAF-1 binding to 40-bp dsRNA.

(H and I) EMSA demonstrating LAF-1 binding to partially duplexed, partially ssRNA with a 5′ tail (H) and 3′ tail (I). Single and double red asterisks denote one and two units of LAF-1-bound bands, respectively.

See also Figure S1.

predicted to be of low complexity and high disorder (Dyson and Wright, 2005; Figures 1D and 1E). The CTD of LAF-1 is composed of many consecutive glycines, FGG boxes, and consecutive glutamines, which is the signature of a prion domain (Taylor et al., 2002; Figure 1D). The FGG box is a hydrophilic-hydrophobic interaction motif mainly found in nuclear membrane-interacting proteins (Suntharalingam and Wente, 2003). Glutamine-rich, low-complexity regions are often found in RNA-interacting proteins, especially in the context of processing bodies or stress granules (Buchan et al., 2008; Gilks et al., 2004). DDX3X also entails a prion-like domain at its CTD, signified by the presence of an FGG box and YGG box, known to be involved in protein-protein assembly (Figure 1E). Despite the presence of several signature sequences and their known function in RNP assembly, the mechanistic details of how the NTD and CTD of LAF-1 and DDX3 may contribute to RNA binding and how such RNA binding may modulate protein conformation (Figure 1F) are unknown. Furthermore, in light of our previous study, which implicates these domains in forming a hub of RNA and proteins during RNP assembly (Elbaum-Garfinkle et al., 2015), questions arise as to how the protein-RNA interaction mode changes as a function of RNA length, protein concentration, and ATP concentration.

To address these questions, here we probed the molecular interaction between LAF-1 and RNA. Using single-molecule fluorescence detection and biochemical measurements, we mapped the changes in protein-RNA binding mode as a function of protein concentration, stoichiometric distribution, RNA length, and ATP concentration. At low concentrations, LAF-1 displayed a stable interaction with ssRNA, where the monomer protein appears to wrap the RNA strand tightly. In contrast, at high concentrations of LAF-1, on a long ssRNA substrate ($\geq$40 nt), multiple units of LAF-1 occupied RNA and induced a dynamic conformational change within the ssRNA. The same concentration-dependent pattern in RNA binding mode was also displayed by DDX3X, raising the possibility of a conserved mechanism shared in this subfamily of RNA helicases. Our mutational analysis indicates that the N-terminal RGG-rich domain lowers the affinity of LAF-1 toward RNA and is directly responsible for inducing the dynamics in RNA, in agreement with our previous finding (Elbaum-Garfinkle et al., 2015). Interestingly, such dynamics lead to accelerated RNA annealing activity, likely reflecting an improved interaction between protein-RNA complexes. In the presence of ATP, the protein-RNA affinity, dynamics, and RNA annealing activity by LAF-1 were all diminished, reflecting a role of ATP in reducing protein-RNA and

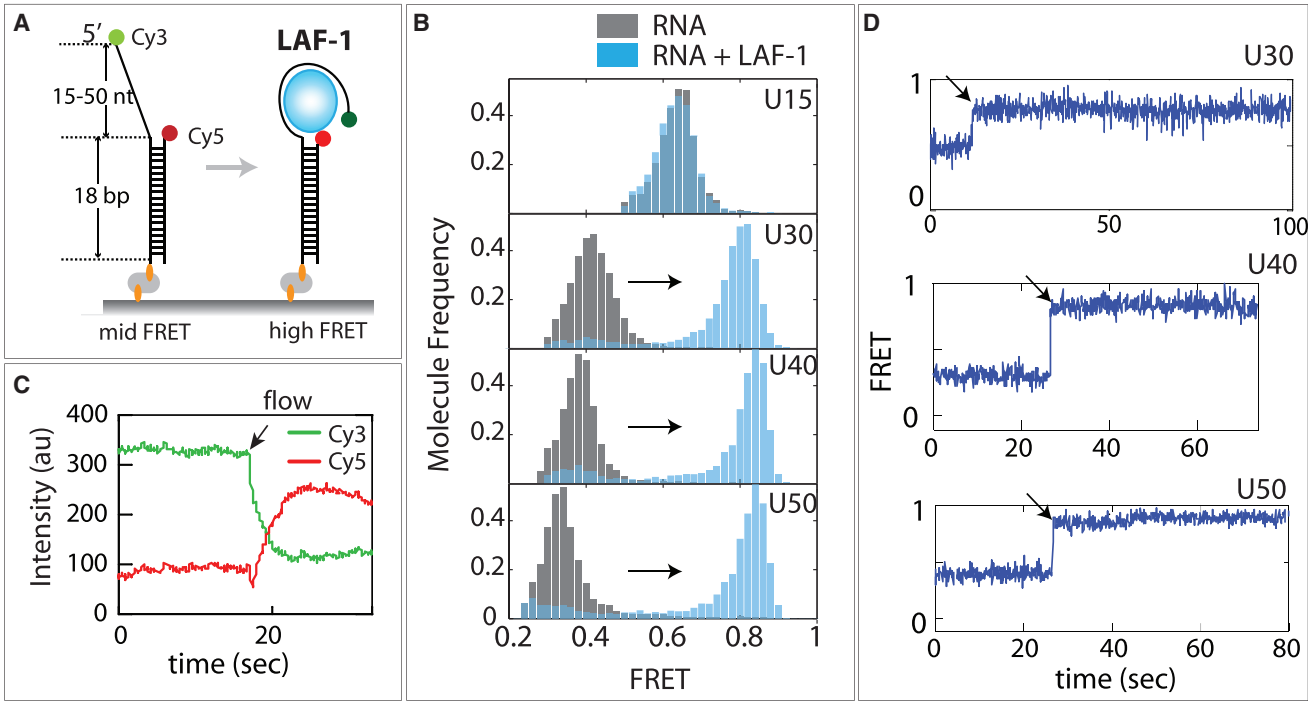

Figure 2. LAF-1 Induces ssRNA Compaction

(A) FRET DNA constructs containing a 5′ U15-50 tail and Cy3/Cy5 dyes across ssRNA.

(B) FRET histograms before (gray) and after (light blue) LAF-1 addition.

(C) Averaged Cy3 and Cy5 intensities obtained from the smFRET experiment. The arrow indicates when LAF-1 was added.

(D) Representative smFRET traces for U30, U40, and U50. A rapid FRET increase occurs immediately after addition of LAF-1 (20 nM).

See also Figures S2 and S3.

protein-protein interactions. Taken together, we propose a model where RNP formation, disassembly, and remodeling are dynamically modulated by parameters such as local protein concentration, length of RNA, and ATP concentration.

RESULTS

ssRNA Compaction by LAF-1

We tested LAF-1 binding to double stranded RNA (dsRNA) and ssRNA substrates by electrophoretic mobility shift assay (EMSA). LAF-1 displayed binding to RNA containing ssRNA at either the 3′ or 5′ end but not to pure dsRNA (Figures 1G–1I). We further confirmed the substrate specificity by single-molecule protein-induced fluorescence enhancement assay (Hwang et al., 2011; Hwang and Myong, 2014), which was consistent with the EMSA data (Figure S1). This substrate specificity is in agreement with a previous structural study of DDX3X (Epling et al., 2015). Based on this finding, we prepared a partially duplexed RNA labeled with Cy3 (donor, green) and Cy5 (acceptor, red) situated at either end of the ssRNA (see Table S1 for the RNA sequence) to probe the conformational change of ssRNA induced by LAF-1 binding by single-molecule Förster resonance energy transfer (smFRET) (Roy et al., 2008). To immobilize this RNA substrate to the single-molecule surface by biotin-NutrAvidin linkage, we constructed biotinylated strands with 15, 30, 40, and 50 nucleotides of polyuracil (poly-U) tail (Figure 2A). We used polyuracil ssRNA rather than mixed bases to avoid the formation of an unintended secondary structure within the ssRNA. We collected FRET values from more than 5,000 molecules and built a FRET histogram for each length of ssRNA. Because of the flexibility of single-strand nucleic acid (Murphy et al., 2004), the resulting FRET values of U15, U30, U40, and U50 ranged between 0.6 (for U15) and 0.3 (for U50) (Figure 2B, gray columns). When LAF-1 protein (20 nM) was applied to this set of ssRNA, we detected a distinct FRET increase for U30, U40, and U50 but not for U15 (Figure 2B, light blue columns). LAF-1 binding to poly-U substrates occurred immediately after the protein addition, as shown in ensemble averaged donor and acceptor intensities (Figure 2C) and in representative single-molecule FRET traces (Figure 2D). This result indicates the following. First, U15 is not long enough for LAF-1 association, but U30–U50 ssRNA can accommodate LAF-1 binding. Second, the discrete FRET shift to a higher level observed in U30–U50 suggests that the end-to-end distance of RNA is diminished in all three substrates. Third, the high FRET peaks remained high even after washing with buffer three times (Figure S2), indicating that the association of LAF-1 with ssRNA is highly stable. In a typical FRET experiment, any protein binding to this type of substrate is expected to occupy space in ssRNA or ssDNA and lower FRET (Hwang et al., 2012, 2014; Qiu et al., 2013). We tested this effect by subjecting an RNA helicase, Sen1, to the U30-FRET RNA construct. The helicase binding to U30

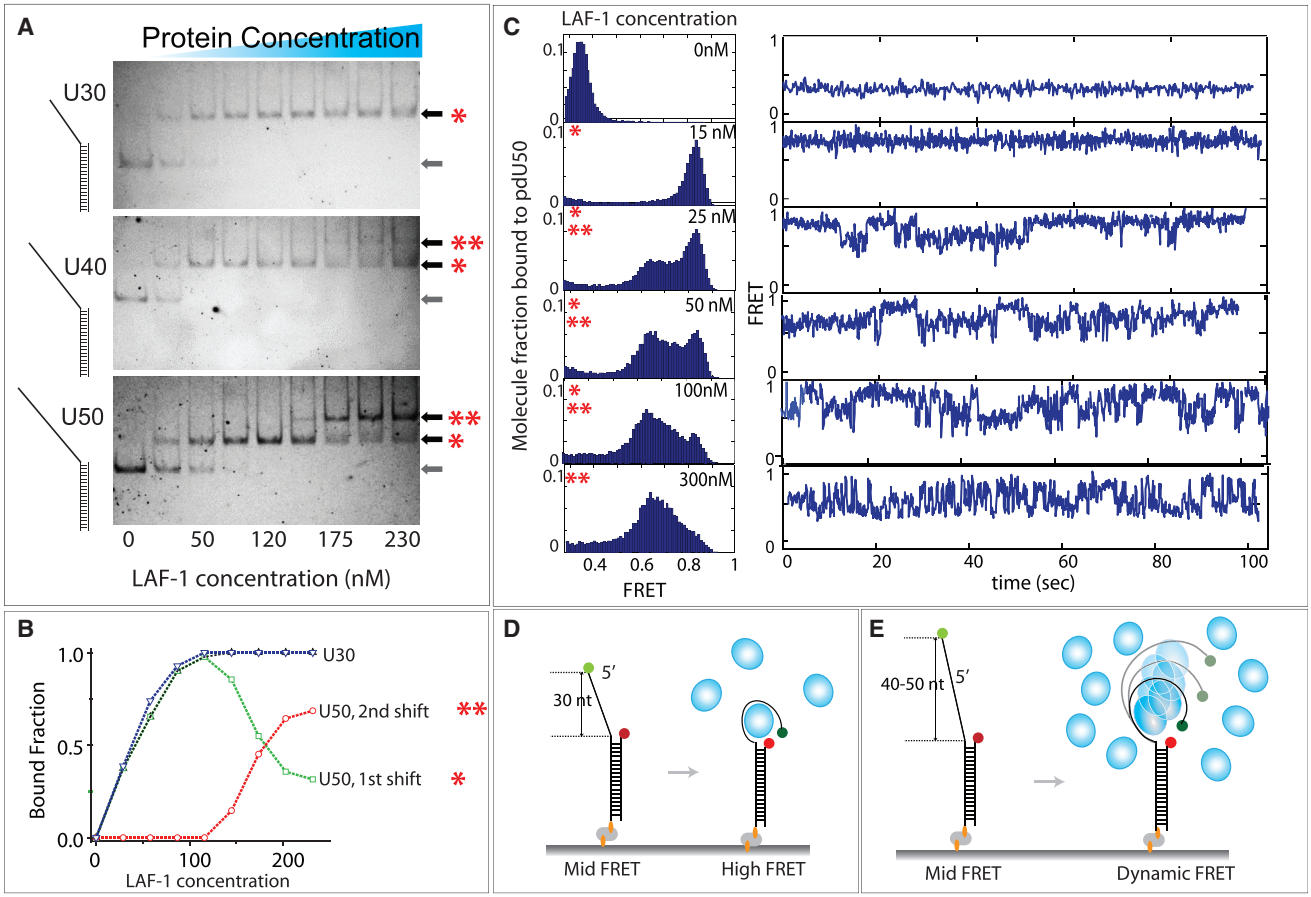

Figure 3. Multimer LAF-1 Induces Dynamic Interaction with ssRNA

(A) EMSA image of U30, U40, and U50 binding to varying concentrations of LAF-1. One and two asterisks denote monomer and multimer status, respectively, and the arrow without any asterisk indicates RNA-only.

(B) Quantitation of the EMSA image for U30 and U50 shown in (A).

(C) FRET histograms and representative smFRET traces for U50 at varying LAF-1 concentrations.

(D and E) Schematics of LAF-1 interaction at low (D) versus high (E) LAF-1 concentrations.

See also Figures S4 and S5.

resulted in a FRET decrease, suggesting that the protein binding increased the dye-to-dye distance by stretching the two ends of the ssRNA (Figure S3). The unusual FRET increase seen here suggests that the protein induces a tight compaction of the flexible ssRNA such that the two dyes are brought to close proximity. The similarly high FRET level obtained for U30, U40, and U50 suggests a length-independent compaction generated by LAF-1.

The Multimer of LAF-1 Induces Dynamic Interaction with ssRNA

We reported earlier that LAF-1 induces dynamics on ssRNA selectively at high concentrations where LAF-1 can self-organize into viscous liquid-like droplets in vitro (Elbaum-Garfinkle et al., 2015). Based on this observation, we hypothesized that LAF-1 may form into multimers/oligomers in this concentration range. To test this effect, we applied varying concentrations (1–230 nM) of LAF-1 to U30, U40, and U50 RNA substrates and performed an EMSA analysis. For U30, only a single band shift appeared throughout all concentrations, whereas U40 and U50 displayed two shifts, denoted by red asterisks, at higher LAF-1 concentrations (Figure 3A). This result clearly shows that shorter ssRNA ($\leq$30 nt) cannot but longer ssRNA ($\geq$40 nt) can accommodate multimers of LAF-1 (Figure 3A). Quantification of the first and second shift obtained for U50 shows that the transition from the first to the second shift occurs at ~100 nM LAF-1 concentration (Figure 3B). We then tested a similar concentration range of LAF-1 in smFRET experiment with U30, U40, and U50. When 15 nM LAF-1 was added to U50 RNA, the low FRET peak shifted completely to a high FRET, again reflecting tight compaction of ssRNA, also observed in Figure 2. When the protein concentrations were raised to 25, 50, and 100 nM, we observed an appearance of a broad mid-FRET peak and diminishing level of the high FRET peak. In agreement, as the protein concentration increased, single-molecule traces displayed a transition from static high FRET to dynamic FRET fluctuation. At 300 nM LAF-1, for U50 RNA, dynamic FRET dominates (Figure 3C). On the contrary, at high LAF-1 concentrations, U30 RNA showed mostly static, non-dynamic high FRET traces.

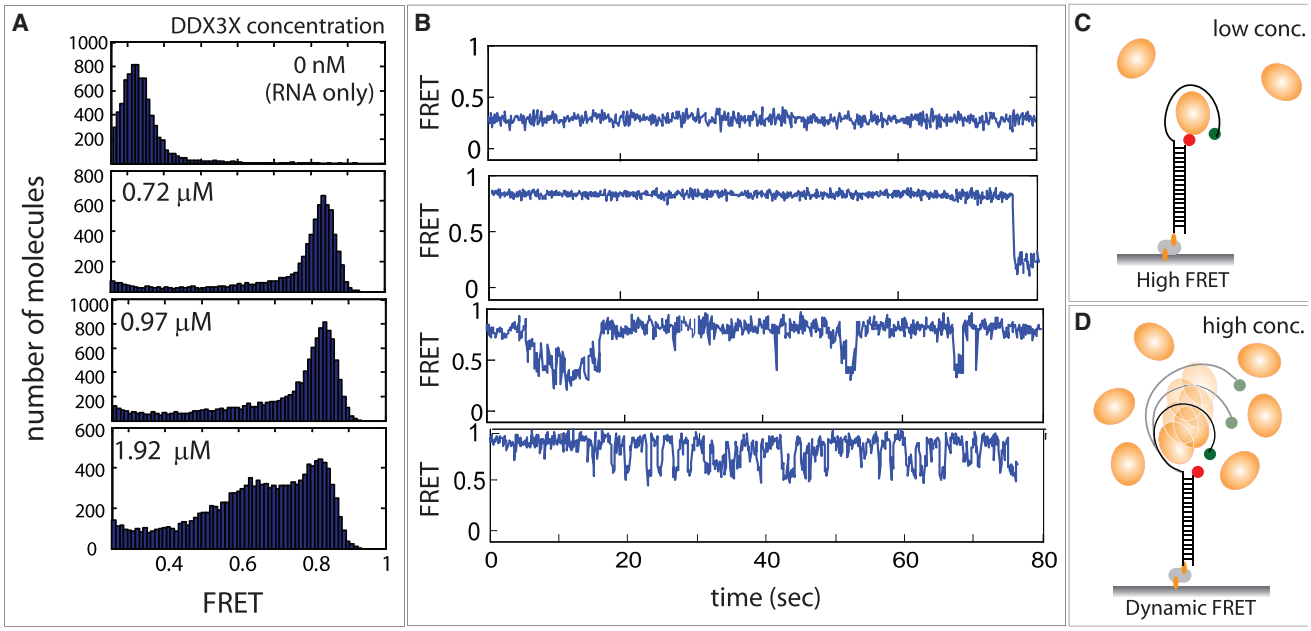

Figure 4. DDX3X Displays Similar Concentration-Dependent Biphasic Behavior as LAF-1

(A) FRET histograms of U50 taken at low to high DDX3X concentrations.

(B) smFRET traces obtained for the conditions in (A).

(C and D) Schematics of DDX3X interaction with ssRNA at low (C) and high (D) DDX3X concentrations.

Based on these results, we interpret that the first band shift in EMSA corresponds to a monomeric LAF-1 that wraps RNA tightly at low concentrations (< 15 nM) (Figure 3D) and that the second shift corresponds to multimers of LAF-1 that induce a dynamic interaction with ssRNA at high concentrations (Figure 3E). We note that FRET fluctuation is not likely due to successive protein binding because the FRET range in the fluctuation (0.45–0.85) is above that of the RNA-only FRET level of 0.35 (Elbaum-Garfinkle et al., 2015). Further examination of smFRET traces obtained for U40 and U50 revealed a small fraction of molecules (10%–15%) exhibiting a two-step FRET increase followed by FRET fluctuation, suggesting that successive binding of two units of LAF-1 may be responsible for the dynamic FRET fluctuation (Figures S4A and S4B). In addition, fluorescently labeled N-terminal domain, which also multimerized (Figure 5E) and exhibited dynamic FRET (Figure 5D), displayed two-step photobleaching, also reflecting two LAF-1-NTD molecules bound to RNA (Figures S4C–S4E).The emerging picture is that the two protein units stay on the RNA and continuously induce dynamic wrapping and unwrapping of RNA. LAF-1 gives rise to static high FRET and dynamic fluctuating FRET, depending on whether it is present as a monomeric or dimeric species, respectively. In the intermediate concentration ranges (25–100 nM), we observed mixed behavior, corresponding to a mixture of monomer and dimer LAF-1 binding to RNA. Thus, the two parameters controlling the static versus dynamic protein-RNA interaction interface are LAF-1 concentration and the length of ssRNA. The tight protein-RNA interface at the monomer state changes to dynamic interaction mode when two units of protein bind RNA together (Figures 3D and 3E).

DDX3X Displays Concentration-Dependent Dynamics on RNA

Based on its high similarity to LAF-1, we prepared DDX3X to test whether it exhibits similar binding behavior to ssRNA. As before, the U50 RNA FRET construct produced a FRET peak at 0.35. Upon addition of DDX3X (720 nM), the low FRET peak shifted to high FRET (~0.8), suggesting a similar tight compaction of ssRNA as observed for LAF-1 (Figure 4A, top). In fact, the high FRET value is similar to what was seen for LAF-1 bound to U50 (Figure 3C, 15 nM), suggesting that a similar mechanism is involved in protein-RNA interaction. As the protein concentration of DDX3X is increased, a broad mid-FRET peak emerges, again in a similar manner as seen in LAF-1 (Figure 4A, bottom). In agreement, the single-molecule traces display a steady high FRET at low DDX3X concentrations and dynamic FRET fluctuation at high concentrations (Figure 4B). In summary, DDX3X induces tight compaction or wrapping of ssRNA at low concentrations (Figure 4C) and imparts dynamic fluctuations in ssRNA at high concentrations (Figure 4D) in a similar manner as exhibited by LAF-1. This result signifies that both LAF-1 and DDX3X undergo the same inherent change in the way they interact with RNA in a concentration-dependent manner.

The N-terminal RGG Domain of LAF-1 Lowers the Affinity to RNA and Induces Dynamics on RNA

We previously reported on the role of N-terminal RGG-rich domains of LAF-1 in inducing dynamics on RNA and promoting droplet formation (Elbaum-Garfinkle et al., 2015). Here we used smFRET and biochemical assays to probe how the intrinsically disordered N- and C-terminal domains of LAF-1 may contribute

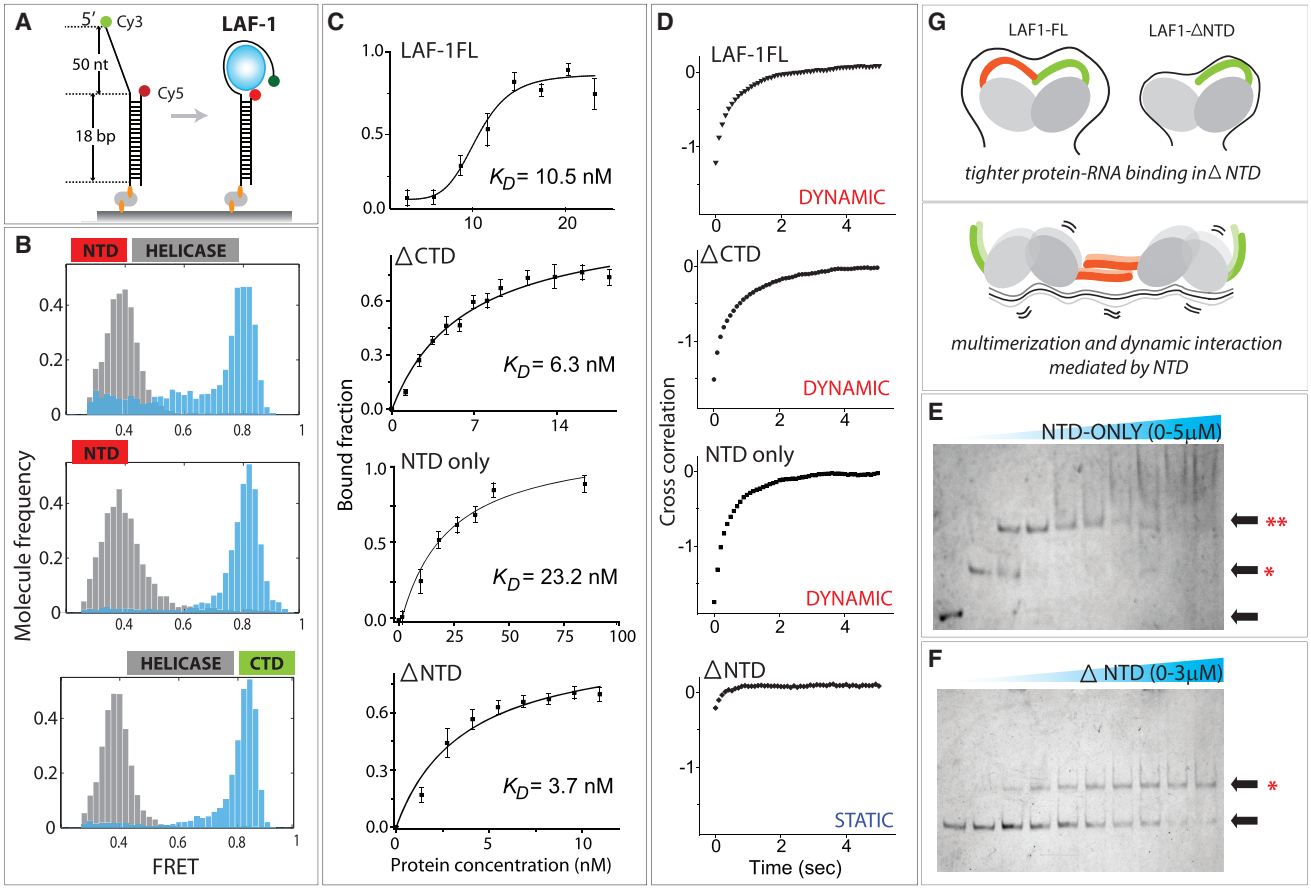

Figure 5. The Role of the RGG-Rich NTD of LAF-1

(A) Schematic of the smFRET experiment for all truncation variants of LAF-1.

(B) FRET histogram before (gray) and after (light blue) LAF-1 addition.

(C) Binding isotherm for LAF-1FL and mutants. All data are represented as mean ± SEM.

(D) Cross-correlation of FRET data for all proteins tested. The strong cross-correlation in LAF-1FL, ΔCTD, and NTD-only results from analysis of FRET fluctuations induced by these proteins. The lack of cross-correlation in the ΔNTD mutant indicates that the NTD is required for the dynamic LAF-1-RNA interaction probed by FRET fluctuation.

(E and F) EMSA of NTD-only (E) and ΔNTD (F). Single and double asterisks denote monomer and multimer status, respectively.

(G) Schematic of the plausible role of the NTD in reducing affinity to RNA while inducing multimer formation and stimulating dynamic interaction with ssRNA.

to RNA binding affinity and dynamics (Figure 5A). We compared three truncation mutants of LAF-1, C-terminal deletion (ΔCTD), N-terminal domain (NTD-only), and N-terminal deletion (ΔNTD) (Figure 5B). On U50, all three LAF-1 protein variants showed a FRET shift to 0.8, suggesting a similar mode of RNA binding and compaction in all cases. Using the fraction of high FRET molecules as binding criteria, we generated a binding isotherm curve for LAF-1FL and the three truncation mutants of LAF-1 (Figure 5C). Interestingly, all three truncation mutants displayed tighter binding to RNA than LAF-1FL, reflecting that both the NTD and CTD negatively regulate RNA binding in the context of full-length LAF-1. When applied at high concentration (2 μM), LAF-1FL, ΔCTD, and NTD-only all exhibited dynamic FRET fluctuation, whereas ΔNTD remained bound in a static manner (Elbaum-Garfinkle et al., 2015). In agreement, the single-molecule FRET data analyzed by cross-correlation displayed a clear presence of FRET fluctuation in all but the ΔNTD mutant (Figure 5D). We asked whether the loss of dynamic interaction with RNA in ΔNTD can be due to its inability to multimerize. To test this effect, we performed EMSA analysis with NTD-only and ΔNTD on U50. Indeed, the result showed that, although the NTD-only mutant multimerized, giving rise to a clear second band shift at low concentration (Figure 5E), the ΔNTD mutant exhibited a single shift throughout the concentration range tested (1–3 μM) (Figure 5F). Based on these findings, we propose a plausible model that defines a role of NTD in modulating protein-RNA interaction. The NTD serves to reduce the protein-RNA affinity, enables multimerization of LAF-1 on long ssRNA, and induces dynamics on RNA (Figure 5G).

Dynamic Interaction Leads to Accelerated RNA Annealing

Next, we asked how the LAF-1 multimer-induced dynamics play a role in RNA remodeling. As in other DEAD box helicases

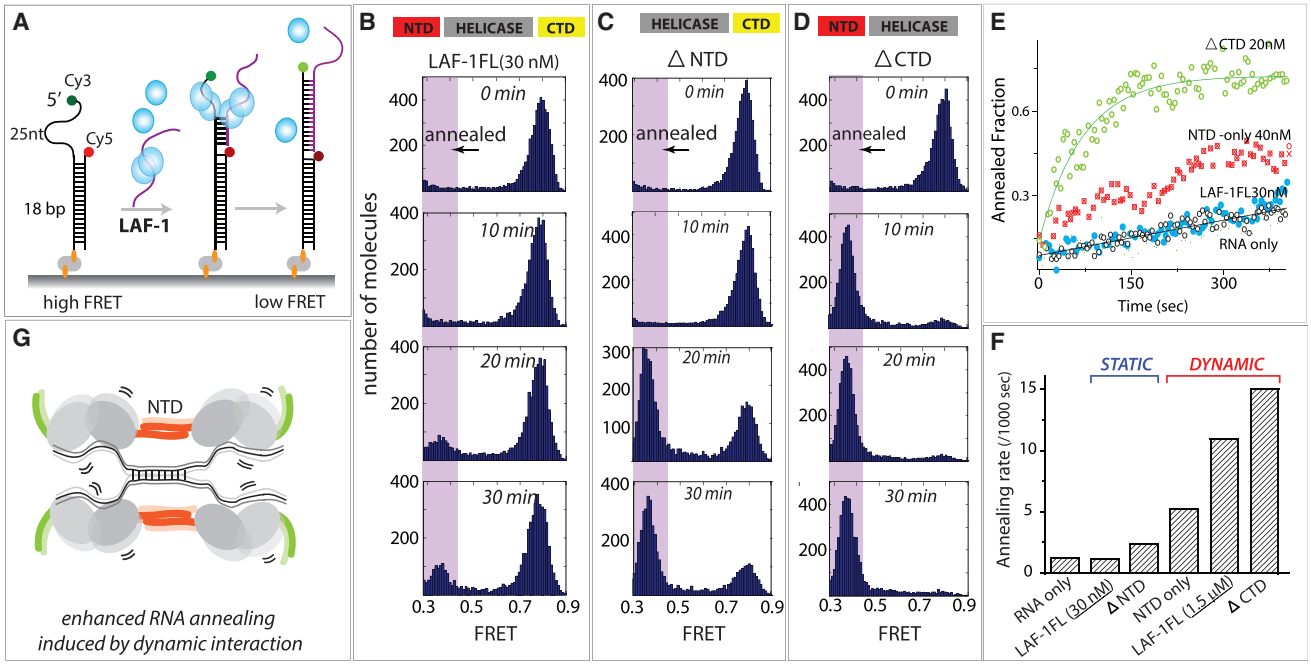

Figure 6. Dynamic LAF-1-RNA Interaction Stimulates RNA Annealing

(A) Schematic of the annealing assay in which high FRET is expected to transition to low FRET upon RNA annealing.

(B–D) FRET histograms obtained for annealing reactions of LAF-1FL (B), ΔNTD (C), and ΔCTD (D). The pink shadow reflects the annealed fraction of molecules.

(E) Annealing reaction of LAF-1, LAF-1FL, and mutants captured in real time.

(F) Annealing rates calculated from (E).

(G) Schematic of NTD-driven dynamics that induce increased interaction between LAF-1-RNA complexes, leading to enhanced RNA annealing.

See also Figure S6.

(Bizebard et al., 2004; Jarmoskaite and Russell, 2011; Linder and Jankowsky, 2011; Rogers et al., 1999; Tijerina et al., 2006), LAF-1 does not lead to active unwinding, as tested by gel electrophoresis and single-molecule fluorescence assays (Figure S5). In light of the correlation between the dynamic interaction of LAF-1 and RNA and the formation of droplets (Elbaum-Garfinkle et al., 2015), we sought to test whether the RNA-protein dynamics can promote efficient RNA annealing by bringing RNP complexes in close proximity. In our single-molecule platform, we immobilized a partially duplexed RNA labeled with FRET dyes at either end of ssRNA, which exhibits high FRET (~0.75) because of the flexibility of ssRNA (Murphy et al., 2004). We note that the FRET value is substantially higher than expected from the 25 polyuracil substrate (U25), likely because of the mixed base composition (with A, U, G, and C) that led to an increased intramolecular interactions within the ssRNA. The same RNA used in the unwinding study revealed the same high FRET (Koh et al., 2014). We applied LAF-1 and ssRNA (10 nM) that bears a complementary sequence to the FRET RNA construct so that annealing will be detected as a decrease in FRET signal (Figure 6A). When the pre-incubated mixture of LAF-1 and 10 nM complementary RNA is applied to a FRET-RNA-immobilized surface, the free LAF-1 is expected to interact with the RNA on the surface, whereas the complementary RNA is already in complex with LAF-1. Therefore, we monitored the annealing induced by interaction among LAF-1-RNA complexes. We tested conditions of no protein (RNA-only), LAF-1FL, ΔNTD, NTD-only, and ΔCTD LAF-1 at a binding isotherm saturation point of 40–60 nM. FRET histograms collected from over 100,000 molecules were plotted over time for LAF-1FL, ΔNTD, and ΔCTD (Figures 6B–6D). The fastest annealing was achieved by the ΔCTD mutant, followed by NTD-only and the wild-type (WT). To obtain the annealing rate, the same FRET histograms were dissected into finer segments from which the fraction of annealed RNA was extracted and plotted (Figure 6E). The calculated annealing rates show that ΔCTD induces the most efficient annealing, with a rate approximately 15 times higher than the RNA-only condition, revealing the CTD of LAF-1 as a negative regulator of RNA annealing activity, possibly by inhibiting interaction between LAF-1-RNA complexes. In contrast, ΔNTD yielded a negligible difference in annealing rate, whereas NTD-only induced a moderate improvement. Wild-type LAF-1 showed a concentration-dependent annealing. When the concentration was low, it barely promoted RNA annealing, but at high protein concentration, it accelerated RNA annealing (Figure S6; Figure 6F). Interestingly, the conditions that promoted dynamic protein-RNA interaction led to an enhanced annealing rate, whereas the two conditions that induced tight compaction of RNA as a monomer (Figures 2 and 4) resulted in no improvement (Figure 6F). This result strongly suggests that the dynamic protein-RNA interaction, mediated by the NTD of LAF-1, is directly responsible for enhanced interaction between LAF-1-RNA complexes, which leads to rapid annealing between two complementary RNA strands (Figure 6G).

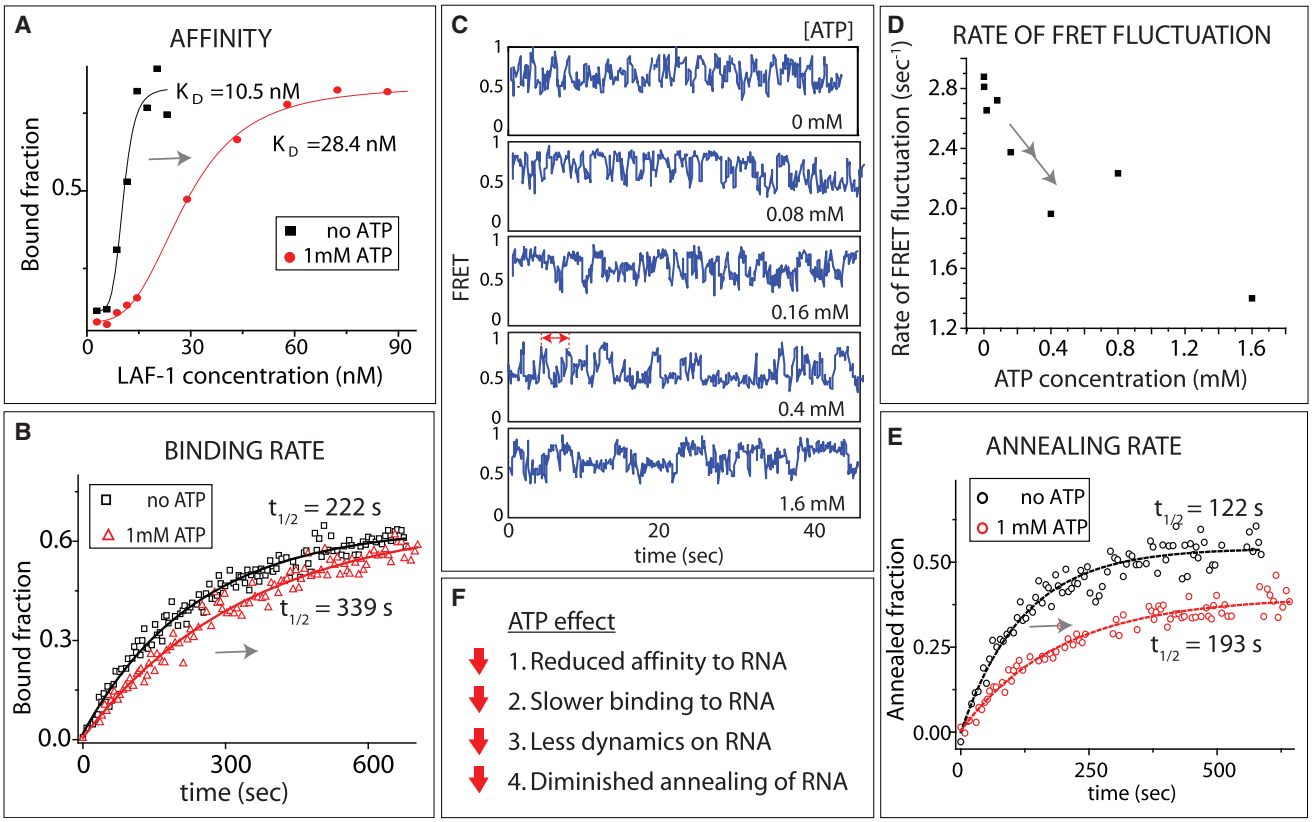

Figure 7. The ATP Effect

(A) Binding isotherm of LAF-1 with and without ATP.

(B) LAF-1 binding rate to U50 with and without ATP.

(C) smFRET traces taken at varying ATP concentrations.

(D) Rate of FRET fluctuations measured at different ATP concentrations.

(E) RNA annealing rate with and without ATP.

(F) Summary of the ATP effect.

See also Figure S7.

ATP Diminishes Protein-RNA Interaction and Dynamics

All of the assays performed and discussed above were done in the absence of ATP. We next asked whether or how ATP might play a role in modulating the interaction between LAF-1 and RNA. First, we examined RNA binding affinity by performing the experiment shown in Figure 2 in the presence of ATP (1 mM). Briefly, the fraction of LAF-1-bound U30 ssRNA molecules that produced high FRET were plotted as a function of LAF-1 concentration. As shown, the binding affinity was reduced by ATP, as evidenced by a higher K_d (Figure 7A). The binding rate of LAF-1 to RNA was calculated by tabulating the LAF-1-bound fraction (high FRET) over time. The difference in half time deduced from the binding kinetic curve reveals that binding is slower in the presence of ATP (Figure 7B). This effect is likely due to ATP hydrolysis, not ATP binding, because ATPγS does not change the binding rate of LAF-1 (Figure S7A). To test whether LAF-1-RNA dynamics may also be influenced by ATP, we applied LAF-1 at a concentration of 1 μM to monitor LAF-1-induced dynamics on ssRNA at varying ATP concentrations. As we increased the ATP concentration, we observed a lower frequency of FRET signal fluctuation (Figure 7C). To quantify this effect, we collected FRET peak-to-peak dwell times from over 200 molecules (Figure 7C, double arrow in red) and plotted the average rate of FRET fluctuation as a function of ATP concentration (Figure 7D). The anti-correlated relationship between the FRET fluctuation frequency and ATP concentration indicates that ATP acts to reduce the dynamic interaction between LAF-1 and ssRNA.

We then sought to test whether the decreased dynamics influence the RNA annealing rate. The annealing experiment performed in the presence and absence of ATP was plotted in the same way as shown in Figure 6E. We applied a 1 μM concentration of LAF-1 so that the annealing outcome would not be controlled by differential binding affinity between the two conditions. In the presence of ATP, the annealing was significantly reduced both in the rate and in the total amount of annealed product (Figure 7E). We note that the result is not affected by limited ATP based on the low rate of ATP hydrolysis by LAF-1 (Figure S7B). This result is consistent with the observation that the dynamic protein-RNA interaction promotes RNA annealing.

In summary, ATP serves to reduce LAF-1's affinity to RNA, decrease its binding rate, lessen the dynamics on RNA, and diminish RNA annealing activity (Figure 7F).

DISCUSSION

Concentration-Dependent Binding Mode

Many studies have reported on protein concentration-dependent unwinding by helicases. For example, the superfamily (SF) 1 helicases Rep, PcrA, and UvrD in *E. coli* and Srs2 from yeast translocate on ssDNA at low concentration, whereas they unwind partially duplexed DNA at an elevated concentration range (Ali et al., 1999; Myong et al., 2005; Park et al., 2010; Qiu et al., 2013). Such results are consistent with the prediction that more than one protein unit is required for efficient unwinding. DEAD box proteins are classified as non-processive helicases because they often display weak unwinding activity limited to a short length of base pairs of RNA (Linder and Jankowsky, 2011; Sengoku et al., 2006). Here we examined LAF-1 and DDX3X, both of which are RNA DEAD box helicases critical for the assembly of RNP granules. Unlike the SF1 helicases, which unwind DNA in a concentration-dependent manner, here we report that LAF-1 and DDX3X exhibit a different RNA binding mode dependent upon protein concentration. At low concentrations (10–20 nM), the monomer unit of the protein wraps ssRNA tightly and stably, as evidenced by a stable high FRET signal that persist even after a buffer wash. The same high FRET value observed in U30, U40, and U50 indicates that the RNA compaction occurs in such a way that the end of the RNA strand comes into close proximity to the ssRNA/dsRNA junction in all RNA substrates. Although we cannot infer the conformational state of RNA, we expect that the multivalent interaction between the protein and RNA enables a tight compaction that may lead to a complete sequestration of RNA. A previous structure of DDX3X revealed an unusual helical element that extends a highly positively charged sequence in a loop that contributed to increased protein-RNA contact (Högbom et al., 2007). Such a structural feature, together with the N- and C-terminal IDR domains, may be responsible for the extensive RNA compaction we observe here. In contrast, a high concentration of LAF-1 allows multimer binding on a long ssRNA substrate and induces continuous and repetitive conformational dynamics on ssRNA, represented by long-lived FRET fluctuations. In light of their function in the assembly of the RNP complex, the compaction of RNA seen at low protein concentrations may represent an inactive or dormant state in which the protein sequesters RNA into its reservoir rather than interacting with neighboring molecules. In contrast, the dynamic interaction obtained at high protein concentrations on a long ssRNA substrate may reflect an activated or charged state in which the dynamic protein-RNA complex actively associates with neighboring protein-RNA components. In this capacity, the dynamic state may reflect a nucleating condition primed for assembly into RNP droplets. Although functionally distinct, such nucleation may be similar to the nucleation event found in Rad51 and RecA (Joo et al., 2006; Qiu et al., 2013), in which a four- to five-monomer cluster represents the active state, which can lead to rapid filament extension suited for homology searching.

Contribution of N- and C-terminal Domains

Both N and C termini of LAF1 consist of IDRs that are composed of elements such as RGG/RG-, G/Q-, and G/S-rich chains of amino acids. These low-complexity domains are expected to contribute to RNA binding and an increased propensity to self-aggregate. Although the NTD of LAF-1 contains RGG-rich segments, which enables RNA binding, the NTD is not solely responsible for the RNA binding affinity of LAF-1 because ΔNTD also exhibits RNA binding. Unexpectedly, ΔNTD displays a higher RNA binding affinity than the full-length protein, suggesting that the NTD reduces RNA binding affinity in the context of the full-length protein. Our results reveal that the NTD of LAF-1 is directly responsible for the concentration-dependent static and dynamic binding modes exhibited by the full-length protein. We propose that the NTD of LAF-1 acts as a switch turned off as a monomer that allows capturing of RNA in a tightly packed format and turned on by forming a multimer that imparts a slippery and fluidic protein-RNA interface and induces dynamic mobility on RNA. The lack of multimerization in ΔNTD strongly suggests that the NTD is directly involved in protein-protein interaction mediated by a long RNA substrate (Figure 5G). Taken together, our result is consistent with a model in which the differing conformation of the NTD between the monomer and multimer dictates its interaction mode with RNA, as depicted in Figure 5G. Although the deletion of the C terminus (ΔCTD) did not induce a drastic change (i.e., the binding affinity and the concentration-dependent static versus dynamic RNA binding), it displayed a significant reduction in RNA annealing activity. We note that CTD-only could not be purified because of heavy precipitation, which likely arose from self-aggregation.

Insights into the RNA Remodeling Function

The core proteins in RNP are expected to exhibit a multifaceted ability to interact with RNA, protein, and RNA-protein (RNP) complexes. First, they bind RNA with high affinity to capture RNA for storage or transport functions. However, such binding cannot be too tight because RNA molecules are required to be dislodged and released as needed for translation, degradation, and transport. Second, the RNP proteins interact with neighboring RNP components to form an organized meshwork to be assembled into granules. Again, the interaction should be strong enough to hold up the constituent and to support further growth of granules but not entirely locked into a rigid structure because the RNP components undergo fluidic exchange with other granules in cells (Jain et al., 2016). Third, they remodel RNA for different purposes. Such activity includes unwinding of duplexed RNA, unfolding of secondary structured regions, annealing of complementary strands, packaging or condensing RNA for storage or transport, and sequestering RNA from degrading enzymes. We demonstrate that LAF-1 does not exhibit unwinding activity but promotes RNA annealing under conditions that induce dynamic RNA-protein interaction (Figure 6F). Interestingly, the same conditions led to phase separation in our previous study (Elbaum-Garfinkle et al., 2015). Based on these findings, the increased annealing activity we observe here may be a proxy for droplet assembly; i.e., a signal informing that the local concentration of protein-RNA complexes has exceeded the threshold required for initiating nucleation for droplet assembly.

Our earlier work demonstrated that LAF-1 forms a liquid-like droplet at physiologically relevant concentration of protein (1 μM) and salt (125 mM NaCl) in the absence of RNA. In the presence of RNA, the droplet exhibits higher dynamics and fluidity, as displayed by microrheology and fluorescence recovery after photobleaching (FRAP) experiments (Elbaum-Garfinkle et al., 2015). Based on these observations, although RNA is not required for the droplet formation, it acts like a fluidizer that may contribute to the dynamic nature of RNP granules in cells. In light of the recent findings of in vitro protein-only droplets developing into a fiber-like state over time (Molliex et al., 2015; Patel et al., 2015), RNA may play a critical role in generating and maintaining the liquid-like property of granules. In addition, the extremely high annealing rate achieved in ΔCTD reveals the role of the CTD in downregulating LAF-1's annealase activity. It could be due to a conformational change of the CTD that results in decreased interaction between protein-RNA complexes.

The Role of ATP and Dynamic Equilibrium in the RNP Complex

In many helicases, ATP binding and hydrolysis lead to catalytic activities such as unwinding, translocation, and protein displacement. Unlike these well-known effects, ATP served to reduce LAF-1's affinity to RNA, diminish the RNA-LAF-1 dynamics, and dampen RNA annealing. If we interpret the high protein-RNA affinity, increased dynamics, and enhanced annealing as the conditions that favor nucleation and assembly of the RNP complex, the ATP-induced effects demonstrated here suggest a condition that promotes disassembly of the RNP complex. In this regard, the ATP concentration, in addition to protein concentration, may be an important parameter that controls the formation and disassembly of LAF-1 RNP granules. A recent study reported a structure of DDX3X bearing an ATP-binding loop (ABL) that is critical for RNA-stimulated ATPase activity. The nuclear magnetic resonance (NMR) chemical shift suggested that the ABL interacts dynamically with ATP (Epling et al., 2015). The weaker protein-RNA interaction in the presence of ATP may arise from such dynamic fluctuation of the ABL-like domain. In agreement, an earlier DDX3X structure was crystallized bound to AMP despite the provided conditions of ATPγS and ADP (Högbom et al., 2007), suggesting that the ATP-bound form is less structured and more flexible. Another structure of a closely related RNA helicase, Vasa, with ATP and RNA exhibited a sharply bent RNA that avoids clashing with the N-terminal domain (Sengoku et al., 2006). This conformation was interpreted to be suited to unwind duplexed RNA by Vasa. In light of our findings, such an arrangement may explain the weakened interaction between the ATP-bound LAF-1 and RNA.

Our results reveal three parameters that can contribute to tuning the RNP assembly and dynamics: the local protein concentration, the length of ssRNA, and ATP. At low protein concentrations, individual LAF-1 units may interact with a single RNA molecule by tightly wrapping it around, perhaps to sequester it from other RNA binding proteins or degrading enzymes. As the local protein concentration increases, more than one LAF-1 occupies single RNA and induces a dynamic interaction interface, which, in turn, triggers enhanced interaction between protein-RNA complexes and improved RNA annealing activity. Such an interaction may be sufficient to drive the nucleation of protein-RNA complexes toward the formation of RNP droplets. In contrast, ATP acts to reduce the affinity and dynamics in LAF-1-RNA interactions, thereby lowering the propensity to assemble the RNP complex. The effect induced by ATP, which appears to favor disassembly of RNP, can represent a critical means to separate and disperse the RNP components to other parts of cytoplasm for delivery or exchange purposes. Our result strongly suggests that ATP acts as a dispersing agent that disaggregates protein-RNA complex formation. Such a role played by ATP can be critical in a crowded cellular environment in which the extremely high protein concentration can easily induce aggregations and pathological inclusions bodies (Lin et al., 2015; Molliex et al., 2015; Patel et al., 2015). The molecular probing of LAF-1 protein to RNA interaction in varying protein concentration, ssRNA length, and ATP reported here presents a plausible mechanism by which RNP complex dynamics can be tuned by several key parameters.

EXPERIMENTAL PROCEDURES

Materials

The vectors pET28a and pUC19 were procured from Novagen and Fisher Scientific, respectively, and *E. coli* strain BL21(DE3) was from Stratagene. Restriction endonucleases, T4 ligase, Taq polymerase, Phusion polymerase, and calf intestinal alkaline phosphatase were purchased from New England Biolabs, and Kapa Taq polymerase was purchased from Kapa BioSciences. Luria broth (LB) powder mix (Luria and Miller broth) and glycerol were from Fisher Scientific, and isopropyl-D-thiogalactopyranoside (IPTG) was from Roche. LB agar plates with antibiotics were obtained from the University of Illinois, Urbana-Champaign (UIUC) cell media center. Custom DNA oligonucleotides were purchased from Integrated DNA Technologies. Materials for DNA purification via agarose gel electrophoresis, including the QIAquick gel extraction kit and Qiaprep Spin miniprep kit were purchased from QIAGEN.

Molecular Cloning

Standard molecular biology protocols were used for cloning. Plasmid DNA was prepared using a miniprep kit (QIAGEN), and vectors were digested by appropriate restriction endonucleases (New England Biolabs). Digested inserts and linearized vectors were purified by a QIAGEN PCR cleaning kit. All molecular sub-cloning steps were performed using *E. coli* strain DH5-alpha and competent cells. The amino acid sequence of LAF1 protein (shown below) was codon-optimized. A codon-optimized, synthesized DNA sequence was inserted to contain 6-histidin at the N terminus. Truncated mutants of LAF1 were generated via PCR with LAF-1-encoding DNA. Phusion high-fidelity polymerase-based PCR reactions (20 μl) were carried out according to the following program: 2 min at 95°C followed by 24 cycles of 15 s each at 95°C, 15 s at the appropriate annealing temperature (gradient range), and 2 min at 72°C. The PCR amplicon encoding for LAF1 was ligated. Positive colonies were selected the next day and amplified, and DNA was sequenced at the UIUC sequencing center.

Protein Expression

The pET28a expression plasmid encoding full-length or deletion mutants of LAF-1 were transformed into *E. coli* expression strain BL21(DE3)pLysS. For protein expression, 10 ml LB culture medium supplemented with 100 μg/l kanamycin was inoculated with a single colony and incubated overnight (16 hr) in an Erlenmeyer flask at 250 rpm, 37°C. Following overnight growth, the culture was diluted 100-fold into 1000 ml LB culture supplemented with 100 μg/l kanamycin. Absorbance was monitored at a wavelength of 600 nm, and, upon reaching an optical density (OD_{600}) of 0.3, protein expression was induced by addition of 1.0 mM IPTG. After incubating cultures at 18°C and 200 rpm for overnight protein expression, cell pellets were harvested by centrifugation (6,000 × *g*, 15 min, 4°C), followed by snap-freezing in dry ice and

ethanol. All amino acid sequences for LAF-1 have been published previously (Elbaum-Garfinkle et al., 2015).

Protein Purification

LAF1 and DDX3X were purified using affinity columns followed by a size exclusion column, as done previously (Elbaum-Garfinkle et al., 2015).

RNA Sample Preparation

All RNA oligonucleotide substrates were purchased from IDT labeled with either Cy3 or Cy5 dyes. The complementary RNA was modified with Cy3 (GE Healthcare) at its 5′ end. RNA substrates were assembled via annealing by mixing Cy3-labeled strand and Cy5-labeled complementary strand RNA at a molar ratio of 1:1 in T100 (10 mM Tris-HCl [pH 7.5] and 100 mM NaCl). The annealing mix was incubated at 65°C for 5 min, followed by slow cooling to room temperature over 3 hr.

Single-Molecule Imaging Buffers

For single-molecule imaging, 1.0 mg/ml glucose oxidase, 0.2% glucose, 2 mM 6-hydroxy-2,5,7,8- tetramethylchromane-2-carboxylic (Trolox), and 0.01 mg/ml catalase were added to the buffer (125 mM NaCl and 50 mM Tris-HCl [pH 7.5]). All FRET and single-molecule imaging measurements were carried out in the same buffer (50 mM Tris-HCl [pH 7.5] and 125 mM NaCl) at room temperature (22 ± 1°C).

Single-Molecule Fluorescence Data Acquisition

Single-molecule fluorescence experiments utilized quartz slides (Finkenbeiner) coated with polyethylene glycol (PEG), prepared as described previously (Roy et al., 2008).

EMSA

Protein-RNA interaction was assayed by EMSA as described (Hellman and Fried, 2007). Briefly, the same Cy3- or Cy5-labeled RNA used for smFRET with Cy3 or Cy5 labeling was utilized. Fluorophore-labeled RNA was diluted to 100 nM and used for the EMSA. For the EMSA, protein and RNA were mixed at the appropriate ratio and incubated at room temperature for 20 min. After incubation, the reaction mixture was mixed with DNA loading dye and subjected to gel electrophoresis (6% polyacrylamide [PAA] gel). The gel was imaged using a Typhoon fluorescence scanner (GE Healthcare).

smFRET Data Analysis

All data analyses were carried out by scripts written in MATLAB, and an additional analysis software was coded in C++ and MATLAB. The software for analyzing single-molecule FRET data is available for download from https://physics.illinois.edu/cplc/software/ and http://vbfret.sourceforge.net/.

Binding Isotherm Calculation

Binding isotherm was calculated from different FRET statuses in different protein concentrations. The fraction of FRET values was counted with the custom MATLAB code. The number of RNAs was also counted to normalize the fraction numbers. The resulting data collection was plotted with Origin 8.0 software using the Hill equation.

SUPPLEMENTAL INFORMATION

Supplemental Information includes seven figures and one table and can be found with this article online at http://dx.doi.org/10.1016/j.molcel.2016.07.010.

AUTHOR CONTRIBUTIONS

Y.K. performed all experiments included in the manuscript. S.M guided the project and wrote the manuscript.

ACKNOWLEDGMENTS

The authors would like to thank Shana Elbaum; Clifford Brangwynne (Princeton University); and Krzysztof Szczepaniak and Christian Eckmann (Martin Luther University) for helpful discussions. Jaya Sarkar proofread the manuscript and Peggy Qiu provided data on Sen1 included in the Supplemental material. This work was supported by the Human Frontier Science Program (RGP0007/2012), American Cancer Society (RSG-12-066-01-DMC), NIH (1DP2GM105453), and National Science Foundation and Physics Frontiers Center Program (0822613) through the Center for the Physics of Living Cells (to Y.K. and S.M.).

Received: March 18, 2016
Revised: May 18, 2016
Accepted: July 15, 2016
Published: August 18, 2016

REFERENCES

Ali, J.A., Maluf, N.K., and Lohman, T.M. (1999). An oligomeric form of E. coli UvrD is required for optimal helicase activity. J. Mol. Biol. *293*, 815–834.

Beckham, C., Hilliker, A., Cziko, A.M., Noueiry, A., Ramaswami, M., and Parker, R. (2008). The DEAD-box RNA helicase Ded1p affects and accumulates in Saccharomyces cerevisiae P-bodies. Mol. Biol. Cell *19*, 984–993.

Bizebard, T., Ferlenghi, I., Iost, I., and Dreyfus, M. (2004). Studies on three E. coli DEAD-box helicases point to an unwinding mechanism different from that of model DNA helicases. Biochemistry *43*, 7857–7866.

Brangwynne, C.P., Eckmann, C.R., Courson, D.S., Rybarska, A., Hoege, C., Gharakhani, J., Jülicher, F., and Hyman, A.A. (2009). Germline P granules are liquid droplets that localize by controlled dissolution/condensation. Science *324*, 1729–1732.

Brangwynne, C.P., Mitchison, T.J., and Hyman, A.A. (2011). Active liquid-like behavior of nucleoli determines their size and shape in Xenopus laevis oocytes. Proc. Natl. Acad. Sci. USA *108*, 4334–4339.

Buchan, J.R. (2014). mRNP granules. Assembly, function, and connections with disease. RNA Biol. *11*, 1019–1030.

Buchan, J.R., Muhlrad, D., and Parker, R. (2008). P bodies promote stress granule assembly in Saccharomyces cerevisiae. J. Cell Biol. *183*, 441–455.

Burke, K.A., Janke, A.M., Rhine, C.L., and Fawzi, N.L. (2015). Residue-by-Residue View of In Vitro FUS Granules that Bind the C-Terminal Domain of RNA Polymerase II. Mol. Cell *60*, 231–241.

Decker, C.J., Teixeira, D., and Parker, R. (2007). Edc3p and a glutamine/asparagine-rich domain of Lsm4p function in processing body assembly in Saccharomyces cerevisiae. J. Cell Biol. *179*, 437–449.

Dyson, H.J., and Wright, P.E. (2005). Intrinsically unstructured proteins and their functions. Nat. Rev. Mol. Cell Biol. *6*, 197–208.

Elbaum-Garfinkle, S., Kim, Y., Szczepaniak, K., Chen, C.C., Eckmann, C.R., Myong, S., and Brangwynne, C.P. (2015). The disordered P granule protein LAF-1 drives phase separation into droplets with tunable viscosity and dynamics. Proc. Natl. Acad. Sci. USA *112*, 7189–7194.

Epling, L.B., Grace, C.R., Lowe, B.R., Partridge, J.F., and Enemark, E.J. (2015). Cancer-associated mutants of RNA helicase DDX3X are defective in RNA-stimulated ATP hydrolysis. J. Mol. Biol. *427*, 1779–1796.

Feric, M., and Brangwynne, C.P. (2013). A nuclear F-actin scaffold stabilizes ribonucleoprotein droplets against gravity in large cells. Nat. Cell Biol. *15*, 1253–1259.

Gilks, N., Kedersha, N., Ayodele, M., Shen, L., Stoecklin, G., Dember, L.M., and Anderson, P. (2004). Stress granule assembly is mediated by prion-like aggregation of TIA-1. Mol. Biol. Cell *15*, 5383–5398.

Goujon, M., McWilliam, H., Li, W., Valentin, F., Squizzato, S., Paern, J., and Lopez, R. (2010). A new bioinformatics analysis tools framework at EMBL-EBI. Nucleic Acids Res. *38*, W695–W699.

Hellman, L.M., and Fried, M.G. (2007). Electrophoretic mobility shift assay (EMSA) for detecting protein-nucleic acid interactions. Nat. Protoc. *2*, 1849–1861.

Högbom, M., Collins, R., van den Berg, S., Jenvert, R.M., Karlberg, T., Kotenyova, T., Flores, A., Karlsson Hedestam, G.B., and Schiavone, L.H.

(2007). Crystal structure of conserved domains 1 and 2 of the human DEAD-box helicase DDX3X in complex with the mononucleotide AMP. J. Mol. Biol. *372*, 150–159.

Hwang, H., and Myong, S. (2014). Protein induced fluorescence enhancement (PIFE) for probing protein-nucleic acid interactions. Chem. Soc. Rev. *43*, 1221–1229.

Hwang, H., Kim, H., and Myong, S. (2011). Protein induced fluorescence enhancement as a single molecule assay with short distance sensitivity. Proc. Natl. Acad. Sci. USA *108*, 7414–7418.

Hwang, H., Buncher, N., Opresko, P.L., and Myong, S. (2012). POT1-TPP1 regulates telomeric overhang structural dynamics. Structure *20*, 1872–1880.

Hwang, H., Kreig, A., Calvert, J., Lormand, J., Kwon, Y., Daley, J.M., Sung, P., Opresko, P.L., and Myong, S. (2014). Telomeric overhang length determines structural dynamics and accessibility to telomerase and ALT-associated proteins. Structure *22*, 842–853.

Jain, S., Wheeler, J.R., Walters, R.W., Agrawal, A., Barsic, A., and Parker, R. (2016). ATPase-Modulated Stress Granules Contain a Diverse Proteome and Substructure. Cell *164*, 487–498.

Jarmoskaite, I., and Russell, R. (2011). DEAD-box proteins as RNA helicases and chaperones. Wiley Interdiscip. Rev. RNA *2*, 135–152.

Joo, C., McKinney, S.A., Nakamura, M., Rasnik, I., Myong, S., and Ha, T. (2006). Real-time observation of RecA filament dynamics with single monomer resolution. Cell *126*, 515–527.

Kato, M., Han, T.W., Xie, S., Shi, K., Du, X., Wu, L.C., Mirzaei, H., Goldsmith, E.J., Longgood, J., Pei, J., et al. (2012). Cell-free formation of RNA granules: low complexity sequence domains form dynamic fibers within hydrogels. Cell *149*, 753–767.

Koh, H.R., Xing, L., Kleiman, L., and Myong, S. (2014). Repetitive RNA unwinding by RNA helicase A facilitates RNA annealing. Nucleic Acids Res. *42*, 8556–8564.

Lin, Y., Protter, D.S., Rosen, M.K., and Parker, R. (2015). Formation and Maturation of Phase-Separated Liquid Droplets by RNA-Binding Proteins. Mol. Cell *60*, 208–219.

Linder, P., and Jankowsky, E. (2011). From unwinding to clamping - the DEAD box RNA helicase family. Nat. Rev. Mol. Cell Biol. *12*, 505–516.

Mattaj, I.W. (1993). RNA recognition: a family matter? Cell *73*, 837–840.

Molliex, A., Temirov, J., Lee, J., Coughlin, M., Kanagaraj, A.P., Kim, H.J., Mittag, T., and Taylor, J.P. (2015). Phase separation by low complexity domains promotes stress granule assembly and drives pathological fibrillization. Cell *163*, 123–133.

Murphy, M.C., Rasnik, I., Cheng, W., Lohman, T.M., and Ha, T. (2004). Probing single-stranded DNA conformational flexibility using fluorescence spectroscopy. Biophys. J. *86*, 2530–2537.

Myong, S., Rasnik, I., Joo, C., Lohman, T.M., and Ha, T. (2005). Repetitive shuttling of a motor protein on DNA. Nature *437*, 1321–1325.

Park, J., Myong, S., Niedziela-Majka, A., Lee, K.S., Yu, J., Lohman, T.M., and Ha, T. (2010). PcrA helicase dismantles RecA filaments by reeling in DNA in uniform steps. Cell *142*, 544–555.

Patel, A., Lee, H.O., Jawerth, L., Maharana, S., Jahnel, M., Hein, M.Y., Stoynov, S., Mahamid, J., Saha, S., Franzmann, T.M., et al. (2015). A Liquid-to-Solid Phase Transition of the ALS Protein FUS Accelerated by Disease Mutation. Cell *162*, 1066–1077.

Qiu, Y., Antony, E., Doganay, S., Koh, H.R., Lohman, T.M., and Myong, S. (2013). Srs2 prevents Rad51 filament formation by repetitive motion on DNA. Nat. Commun. *4*, 2281.

Reijns, M.A., Alexander, R.D., Spiller, M.P., and Beggs, J.D. (2008). A role for Q/N-rich aggregation-prone regions in P-body localization. J. Cell Sci. *121*, 2463–2472.

Rogers, G.W., Jr., Richter, N.J., and Merrick, W.C. (1999). Biochemical and kinetic characterization of the RNA helicase activity of eukaryotic initiation factor 4A. J. Biol. Chem. *274*, 12236–12244.

Roy, R., Hohng, S., and Ha, T. (2008). A practical guide to single-molecule FRET. Nat. Methods *5*, 507–516.

Sengoku, T., Nureki, O., Nakamura, A., Kobayashi, S., and Yokoyama, S. (2006). Structural basis for RNA unwinding by the DEAD-box protein Drosophila Vasa. Cell *125*, 287–300.

Shih, J.W., Wang, W.T., Tsai, T.Y., Kuo, C.Y., Li, H.K., and Wu Lee, Y.H. (2012). Critical roles of RNA helicase DDX3 and its interactions with eIF4E/PABP1 in stress granule assembly and stress response. Biochem. J. *441*, 119–129.

Sigrist, C.J., de Castro, E., Cerutti, L., Cuche, B.A., Hulo, N., Bridge, A., Bougueleret, L., and Xenarios, I. (2013). New and continuing developments at PROSITE. Nucleic Acids Res. *41*, D344–D347.

Suntharalingam, M., and Wente, S.R. (2003). Peering through the pore: nuclear pore complex structure, assembly, and function. Dev. Cell *4*, 775–789.

Taylor, J.P., Hardy, J., and Fischbeck, K.H. (2002). Toxic proteins in neurodegenerative disease. Science *296*, 1991–1995.

Tijerina, P., Bhaskaran, H., and Russell, R. (2006). Nonspecific binding to structured RNA and preferential unwinding of an exposed helix by the CYT-19 protein, a DEAD-box RNA chaperone. Proc. Natl. Acad. Sci. USA *103*, 16698–16703.

Updike, D., and Strome, S. (2010). P granule assembly and function in Caenorhabditis elegans germ cells. J. Androl. *31*, 53–60.

Wippich, F., Bodenmiller, B., Trajkovska, M.G., Wanka, S., Aebersold, R., and Pelkmans, L. (2013). Dual specificity kinase DYRK3 couples stress granule condensation/dissolution to mTORC1 signaling. Cell *152*, 791–805.

Yarunin, A., Harris, R.E., Ashe, M.P., and Ashe, H.L. (2011). Patterning of the Drosophila oocyte by a sequential translation repression program involving the d4EHP and Belle translational repressors. RNA Biol. *8*, 904–912.

Zhang, H., Elbaum-Garfinkle, S., Langdon, E.M., Taylor, N., Occhipinti, P., Bridges, A.A., Brangwynne, C.P., and Gladfelter, A.S. (2015). RNA controls PolyQ protein phase transitions. Mol. Cell *60*, 220–230.